Available online at www.sciencedirect.com
SCIENCE DIRECT
Earth and Planetary Science Letters 243 (2006) 26–43
EPSL
www.elsevier.com/locate/epsl

Isotopic outcomes of N-body accretion simulations: Constraints on equilibration processes during large impacts from Hf/W observations

F. Nimmo *, C.B. Agnor

Department of Earth Sciences, University of California Santa Cruz, Santa Cruz, CA 95064, United States

Received 12 August 2005; received in revised form 3 December 2005; accepted 12 December 2005
Available online 7 February 2006
Editor: S. King

Abstract

Most estimates of planetary core formation timescales using hafnium–tungsten (Hf–W) isotopes employ analytical expressions assuming either continuous planetary growth or instantaneous core formation. In contrast, dynamical modelling of planetary accretion suggests that the final stage of terrestrial planet formation is punctuated by multiple large and stochastic impacts. Such giant impacts have significant thermal and isotopic consequences. We present a framework for calculating the Hf–W isotope evolution of individual bodies based on the results of an N-body accretion simulation and assuming constant partition coefficients. The results show that smaller bodies exhibit a larger range in isotopic values than larger bodies, because the latter have suffered more impacts. The analytical core formation timescales calculated using these isotopic values can differ very significantly from the timing of the final giant impact each planet actually experiences. Simulations in which 1) even the largest impactors undergo re-equilibration with the target's mantle, rather than the cores merging directly, and 2) the original planetary embryos possessed radially variable iron : silicate ratios, produce results which are consistent with the observed physical and isotopic characteristics of inner solar system bodies. Varying W partition coefficients (due to changing mantle oxidation state) or initial planetesimal Hf/W ratios might produce similar isotopic outcomes, and potentially permit core mergers without violating the isotopic constraints. The style of re-equilibration required suggests that magma oceans were present on Mars-sized and larger bodies; an alternative for bodies of Mars-size and smaller is that the bulk of the mass was delivered as impactors much smaller than the target. For Mars we conclude that a prolonged (~10 Myr) accretion process is both dynamically and isotopically plausible. We also predict likely Pd–Ag isotopic anomalies for Vesta-, Mars- and Earth-size bodies.

Keywords: accretion; isotope; hafnium; tungsten; impact; equilibration

1. Introduction

The divergent evolutionary paths taken by the terrestrial planets are substantially a result of the initial conditions established by their growth from numerous smaller planetesimals. Understanding the details of the accretionary process is thus an important step in understanding present-day solar system diversity. There are two indirect methods of investigating the late stages of terrestrial planet formation: dynamical simulations of the accumulation process ([1,2], e.g.); and isotopic observations, especially of the hafnium–tungsten (Hf–W) system, ([3–5], e.g.). Both methods of investigation can

* Corresponding author.
E-mail address: fnimmo@es.ucsc.edu (F. Nimmo).

0012-821X/$ - see front matter © 2005 Elsevier B.V. All Rights reserved.
doi:10.1016/j.epsl.2005.12.009

provide constraints on the formation timescales of the planets. In this paper, we present a framework for performing isotopic evolution calculations using the collision histories generated by simulations of planetary accretion, which typically include several late, large impacts. Doing so allows us to use both physical (e.g. mass, semi-major axis) and isotopic constraints to distinguish between different accretion scenarios. In particular, here we examine the effect of compositional heterogeneity and different isotopic equilibration styles on the resulting isotopic signatures produced, making the simplifying assumption that partition coefficients remain constant. We conclude that the observed physical and isotopic characteristics of inner solar system bodies are consistent with our dynamical simulations if 1) even the largest impactors undergo re-equilibration with the target's mantle and 2) the original planetary embryos possessed radially variable iron : silicate ratios.

The accretion of the terrestrial planets consists of several distinct stages ([6–9], e.g.). Accretion of the initial dusty protoplanetary disk by runaway growth into lunar-to Mars-sized planetary embryos is probably complete within ≈1 Myr of solar system formation ([10–13], e.g.). The final stage of planet accretion involves giant impacts between these planetary embryos, a process typically requiring $\mathcal{O}(10^8)$ yr. This late stage has been modeled extensively using Monte Carlo methods [14] and direct integrations ([1,15], e.g.). It is this final stage that we will focus on.

Several isotopic systems have half-lives comparable to the timescale for late-stage accretion, and can therefore potentially provide a record of the events which occur during this period. The most-studied system, which we will focus on, is Hf–W, but similar systems (e.g. ^{97}Tc–^{97} Mo [16], ^{107}Pd–^{107} Ag [17]) also exist which may provide additional constraints in future.

The importance of the Hf–W system is that Hf is lithophile (it becomes concentrated in silicates when differentiation occurs) while W is siderophile and thus becomes concentrated in the core. Unstable ^{182}Hf decays to ^{182}W with a half-life of 9 Myr. Thus, core formation while live ^{182}Hf exists will result in subsequent ingrowth of ^{182}W in the mantle. The resulting ratio of ^{182}W to the stable isotopes ^{183}W and ^{184}W will thus be higher than the ratio for chondritic objects which have never differentiated; that is, the mantle develops a ^{182}W excess. The earlier the core formation event, the larger the excess ^{182}W. Thus, measuring the ^{182}W excess in the mantle places a constraint on the timing of core formation.

There is now broad agreement about the existence of W isotopic anomalies for Vesta, the Moon and, after some initial confusion on the correct chondritic isotopic ratio ([18], e.g.), the Earth and Mars [19–21]. These results have been interpreted as indicating relatively early core formation (<50 Myr), with smaller objects generally having cores which formed earlier. Interpreting the data, however, depends on the particular model adopted for the process of core formation. Analytical models typically assume either a single core-forming event, or a smooth increase in body mass with time. These assumed growth scenarios are very different from those produced by late stage accretion models which show that much of a body's mass can be delivered by a few, large impacts which occur in a highly stochastic manner.

Recently, two important papers have calculated isotopic effects based on more realistic planetary growth models derived from N-body simulations [4,5]. The approach presented here builds on these works, but differs in three respects. Firstly, we track the isotopic evolution of every body, with the result that collisions can have different isotopic outcomes depending on the prior characteristics of the colliding bodies ([22], c.f.). Secondly, because each body has a definite initial location in space, we can also examine the effect of initial spatial variations in characteristics (such as core mass fraction or volatile abundance) on the isotopic outcome. Finally, by examining the results from a suite of different accretion models, we are able to address the variability introduced by the stochastic nature of the accretion process.

The remainder of the paper is organized as follows. We begin (Section 2) with a brief discussion of the physical and chemical consequences of large impacts (so far as they are understood) to justify the initial conditions and different re-equilibration models we subsequently adopt. We then (Section 3) describe the isotopic calculations, and provide some details of the N-body simulations on which they are performed. Section 4 describes the results obtained, and compares the outcomes with the characteristics of Mars, Vesta and the Earth. Section 5 draws some general conclusions and suggests further questions which need to be answered.

2. Initial conditions and re-equilibration during impacts

It is generally thought that Moon- to Mars-sized planetary embryos accumulate via runaway growth within the first few million years of solar system formation ([10–13], e.g.). This growth stage typically involves impactors which are much smaller than the target embryos. The late stage of terrestrial planet formation begins as these embryos begin to perturb each other to crossing orbits where they suffer a series of giant collisions en route to

forming the larger planets. As we show later (Section 4.1), the initial state of these embryos (whether or not they are already differentiated) has a significant effect on their subsequent isotopic evolution. The differentiation state of an embryo in turn depends on its prior thermal evolution. If temperatures become high enough that melting occurs, differentiation is highly probable [23], although it depends on various complicating factors such as the melt fraction [24], the dihedral angle of iron–silicate melts [25], and the degree of shear [26].

A significant source of heat is the gravitational energy released during runaway growth. Unfortunately, as discussed below, the uncertainties are such that it is unclear whether or not Mars-sized objects are likely to have undergone differentiation due to gravitational energy alone [27]. Live ^{26}Al, if present, is sufficiently energetic to cause widespread melting [28,29], but has a half-life of only 0.7 Myr and may thus have decayed before embryo formation was complete. The Eucrite Parent Body (often assumed to be Vesta), however, did differentiate when ^{26}Al was present, that is, within ≈3 Myr of solar system formation [30]. Isotopic data (especially ^{182}W, ^{107}Pd–^{107} Ag and ^{53}Mn–^{53} Cr) in iron meteorites are also consistent with a similarly early core formation event ([31–33], e.g.). It therefore seems likely that at least some of the embryos were differentiated prior to their involvement in the final stage of accretion. In our models below we adopt end-member models in which either all planetesimals start undifferentiated, or they all differentiate at a particular time. In reality, the situation is likely to be an intermediate case, since growth (and hence differentiation) will take place at different rates depending on heliocentric distance [34].

The final stage of accretion begins at different times at different heliocentric distances, is prolonged (up to ~100 Myr), and involves impacts between bodies of Mars-size or greater. Such impacts can result in heating and melting, with the effects depending strongly on the masses of the objects involved. A simple calculation [35] gives an expected temperature rise ΔT due to gravitational potential energy release of

$$\Delta T \approx \frac{3}{5} f \left(\frac{4\pi\rho}{3}\right)^{1/3} \frac{GM^{2/3}}{C_p} = 38,000K \left(\frac{M}{M_e}\right)^{2/3} f \quad (1)$$

where M and ρ are the final mass and mean density of the object, M_e is the mass of the Earth, C_p is the specific heat capacity and G is the universal gravitational constant. The factor f ($0<f<1$) is determined by the efficiency of the conversion of kinetic and gravitational into thermal energy following the impact [36–38]. This factor is essentially unknown, and probably depends in a complicated fashion on the relative sizes of the two bodies, their initial conditions and the impact geometry [35]. It is clear, however, that an impact resulting in an Earth-sized body will result in massive melting [39]. On the other hand, a Mars-sized body ($M/M_e \approx 0.1$) might well avoid global melting, especially if $f \leq 0.1$. Because the collisions in our simulations typically result in planetary masses $>0.1\ M_e$, we will generally assume that any undifferentiated object undergoes differentiation on collision (see below). We later relax this assumption to investigate what changes occur if small impacts do not lead to differentiation (Section 4.2).

The physical consequences of the impact process have important, but very poorly understood, chemical implications [23,40–42]. As is evident from the different conclusions reached by [4] and [5] regarding the Moon-forming impact, different assumptions about re-equilibration during collisions can lead to significantly different conclusions concerning accretion histories (see also [3]). One of the aims of this work is to investigate which re-equilibration scenarios are most consistent with the observations.

Ultimately, isotopic re-equilibration requires that the iron and silicate phases be mixed at lengthscales small enough that diffusion can take place. Re-equilibration therefore depends on the (phase- and temperature-dependent) diffusivity and characteristic distance between the two phases. Unfortunately, computational simulations of large impacts provide only limited information on either of these factors. Even the highest resolution codes typically consider particles of order 100 km radius [43], while diffusive transport in liquid materials is expected to be important only on centimetric lengthscales [23].

Collisions in which the impactor is much smaller than the target result in vapourization of the impacting material [44]. In this case, the material will be completely re-equilibrated with the target's mantle (and the core material will segregate later). A somewhat larger impactor striking a deep magma ocean is likely to suffer a similar fate [42]: the impactor will be sufficiently disrupted that re-equilibration is rapid compared to the transit time for core material.

However, it is possible that the chemical effects of the largest impacts (such as the Mars-sized impactor invoked for Moon formation) are fundamentally different [45,46]. Rubie et al. [42] suggest that re-equilibration will take place unless the impactor core size is comparable to the magma ocean depth. Harper and Jacobsen [45] observe that the SPH models of Cameron and Benz [47] also suggest accretion without re-equilibration; however, more recent models [43] have been used to argue the opposite [5].

The rapidity of impactor core segregation during a giant impact may well depend, like other processes, on the details of the collision geometry [48], making it hard to generalize. Furthermore, not only are the impact simulations far too coarse to investigate such processes, but artifacts may also arise because such simulations do not treat viscosity with any realism. Most impact simulations include artificial viscosity for handling shocks, which can behave like a numerics-dependent physical viscosity [49]. It may be possible to place crude constraints on likely iron droplet sizes from scaling arguments [23], but our current understanding of the microphysics of giant impact events is very limited.

As a result, there is no agreement on the likely isotopic effects of the largest impacts [4,5]. In the absence of a good physical understanding of the processes governing re-equilibration, we therefore investigate several different re-equilibration scenarios. By comparing the results with observations, we can narrow down the range of plausible scenarios, and thereby place some constraints on the physical processes likely to be operating.

3. Methods

Here we describe our methods in some detail, for those unfamiliar with isotopic calculations. A key reference for the following is [45]; while these authors use isotopic ratios, for computational purposes it is clearer and more convenient to work with primitive variables, principally mass and elemental concentration. A similar but more sophisticated treatment than the one presented here has recently been published by [5].

Two physical processes are responsible for the isotopic anomalies generated during core formation. The first is fractionation; the second is radioactive decay. If fractionation occurs while the radioactive (parent) element is still extant, isotopic anomalies result due to the subsequent ingrowth of the daughter element (e.g. ^{182}W) in the mantle (which has high Hf/W). These anomalies can be detected at the present day.

Regarding fractionation, some elements partition into silicates during differentiation (e.g. Hf), others prefer metals (e.g. W). Here we will define the partition coefficient D^{i} of element i as

$$D^{\mathrm{i}} = \frac{C^{\mathrm{i}}_{\mathrm{m}}}{C^{\mathrm{i}}_{\mathrm{c}}} \tag{2}$$

where $C^{\mathrm{i}}_{\mathrm{m}}$ is the concentration of element i in the mantle, and $C^{\mathrm{i}}_{\mathrm{c}}$ that in the core. Note that this definition of D^{i} is the inverse of that of [50]. A practical advantage of using partition coefficients is that they may depend on pressure, temperature and other factors such as oxidation state [51,50]. Explicit use of these variables makes incorporating such dependencies more straightforward.

For the case of an initially homogeneous object which differentiates into core and mantle, mass balance considerations and the definition of D^{i} give

$$C'^{\mathrm{i}}_{\mathrm{m}} = \frac{C^{\mathrm{i}}}{y + \frac{(1-y)}{D^{\mathrm{i}}}}, C'^{\mathrm{i}}_{\mathrm{c}} = \frac{C^{\mathrm{i}}}{1 + y(D^{\mathrm{i}} - 1)} \tag{3}$$

Here C^{i} and C'^{i} are the concentrations of the element i before and after differentiation, respectively, y is the silicate mass fraction (y may vary from body to body), and the subscripts m and c refer to core and mantle as before. Thus, as one would expect, a large value of D implies an element is found mainly in the mantle, and vice versa. We will generally assume a constant value for D, though this may be relaxed if desired.

As discussed above, the isotopic signature of an impact is determined by the degree to which re-equilibration occurs [3,4,5,46,52]. Here we will focus initially on two end-member re-equilibration scenarios, and discuss more realistic intermediate cases in Section 4 below. One end-member is the "primitive differentiation" model of [52] (Fig. 1a). In this hypothesis, if the impactor is undifferentiated, it differentiates on impact and fractionates according to Eq. (3). For our numerical simulations, we assume that the target body also differentiates on impact if it has not already done so. Following impact, the cores and mantles of the two bodies are then added together without further equilibration, and the resulting isotopic anomalies determined from the mass-weighted average. For instance, the resulting mantle concentration of species i after the merger is given by

$$C^{\mathrm{i}}_{\mathrm{m}} = \frac{C^{\mathrm{i}}_{\mathrm{m},1} y_1 M_1 + C^{\mathrm{i}}_{\mathrm{m},2} y_2 M_2}{y_1 M_1 + y_2 M_2} \tag{4}$$

and similarly for the core. Here y is the silicate mass fraction in each body, M is the total mass and the subscripts 1 and 2 refer to the two bodies prior to collision. The resulting silicate mass fraction of the final body is given by

$$y = \frac{y_1 M_1 + y_2 M_2}{M_1 + M_2}. \tag{5}$$

This "primitive differentiation" model as originally posed is probably most appropriate to stages of accretion when the impactor and target are comparable in mass.

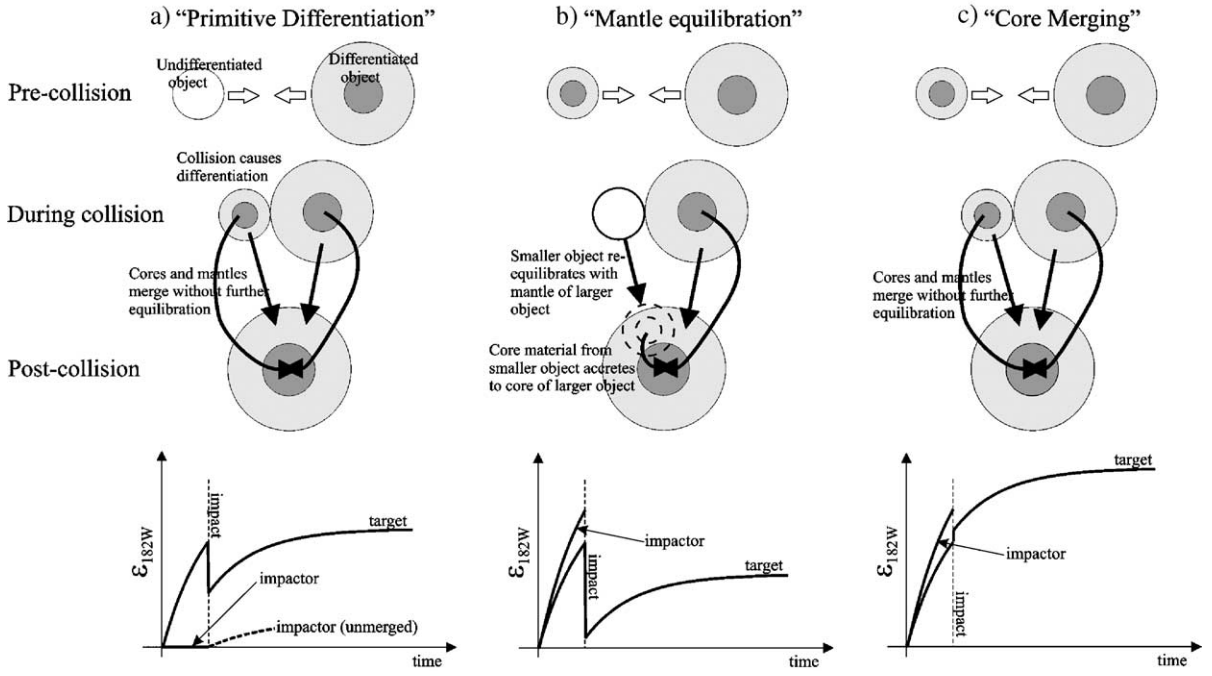

Fig. 1. Schematic outlines of three main re-equilibration scenarios discussed in the text (c.f. [45,52]). We generally assume that the larger body (target) differentiates upon impact if it has not already done so. The lower panels give schematic depictions of the evolution of mantle tungsten anomalies for the target and impactor under each re-equilbration scenario (see text). If the target and impactor are similar sizes, A or C are favoured; if the sizes are very different, B is likely.

The second end-member scenario is termed the "mantle equilibration" scenario (Fig. 1b). Again, we assume that the impact causes the larger object (target) to differentiate, if it has not already done so. The core and mantle of the impactor then re-equilibrate completely with the mantle of the target, and only then does the core material separate out. This re-equilibration drives the mantle isotopic signature downwards. The mantle concentration following re-equilibration of the impactor (body 2) is calculated using an approach similar to Eq. (4):

$$C_{\mathrm{m}}^{\mathrm{i}} = \frac{C_{\mathrm{m},1}^{\mathrm{i}} y_1 M_1 + C_2^{\mathrm{i}} M_2}{y_1 M_1 + M_2} \tag{6}$$

Here C_2^{i} is the bulk concentration (core plus mantle) of element i in body 2. The core and mantle concentrations following the separation of the core material from body 2 are given by Eq. (3). In this instance y is calculated using Eq. (5) but with the denominator given by $y_1 M_1 + M_2$ (because the core of body 1 is not involved).

This kind of scenario is appropriate if the impactor is much smaller than the target, in which case the impactor material will be thoroughly re-equilibrated with the target's mantle. Whether a large body impacting into a magma ocean also results in such re-equilibration is poorly understood (see Section 2 above). An alternative possibility [4] is that very large impacts may result in the cores and mantles merging without any significant equilibration (Fig. 1c). In this case, the resulting concentrations are governed by Eq. (4). Note that this core-merging scenario is identical to a "primitive differentiation" scenario in which both colliding objects have already differentiated. Under the core merging scenario, two equal bodies would collide without generating any isotopic record of their collision [5].

Eqs. (2)–(6) may be applied to any element. However, the importance of the Hf/W system is that ^{182}Hf is unstable, and decays to ^{182}W:

$$\begin{aligned} C^{182\mathrm{Hf}} &= C_0^{182\mathrm{Hf}} \exp(-\lambda t), \\ C^{182\mathrm{W}} &= C_0^{182\mathrm{W}} + C_0^{182\mathrm{Hf}} (1 - \exp(-\lambda t)) \end{aligned} \tag{7}$$

Here $C^{182\mathrm{Hf}}$ and $C_0^{182\mathrm{Hf}}$ are the current and initial ($t=0$) concentrations of Hf, respectively (likewise for W), λ is the decay constant ($=0.077$ Ma^{-1}) and time is measured forwards from solar system formation. Accordingly, the concentrations of ^{182}Hf and ^{182}W evolve with time, irrespective of any other process.

Applying these equations to the results of an accretion code is relatively straightforward. Each body may be represented by its mass and eight values, representing

the concentrations of ^{182}Hf, ^{182}W and the stable elements ^{180}Hf and ^{183}W in the core and mantle, respectively. For a timestep in which no other process occurs, these values may be updated using Eq. (7). If an impact does occur, depending on the assumed style of equilibration Eqs. (3)–(5) or their equivalents are used to update the isotopic concentrations. An important point is that these calculations may be carried out as a post-processing step on the output from N-body simulations, since the isotopic evolution is assumed to have no influence on the orbital dynamics.

Here we define the tungsten isotope anomaly, ϵ_{182W} (or just tungsten anomaly), using the approach of [45]

$$\epsilon_{182W} = \left[\frac{(C^{182W}/C^{183W})}{(C^{182W}/C^{183W})_{CHUR}} - 1\right] \cdot 10^4 \quad (8)$$

where CHUR refers to the undifferentiated (chondritic) ratio. Converting the model results to this measure is trivial: it simply requires the isotopic evolution of one additional chondritic particle (which never differentiates) to be tracked.

Another important parameter is the mantle Hf/W fractionation factor $f^{Hf/W}$

$$f^{Hf/W} = \frac{(C^{180Hf}/C^{183W})}{(C^{180Hf}/C^{183W})_{CHUR}} - 1 \quad (9)$$

where $(C^{180Hf}/C^{183W})_{CHUR} = 2.836$, following Jacobsen [5]. The importance of this parameter is that variations in the mantle Hf/W ratio will lead to variations in ϵ_{182W}. The fractionation factors for the core and mantle may be directly related to D^{Hf} and D^{W} if y is known [45].

Fig. 1 gives a schematic illustration of the evolution of ϵ_{182W} under the different re-equilibration scenarios. In Fig. 1a, the target differentiates at time $t=0$ and its mantle evolves towards a positive ϵ_{182W} value with time, while the impactor is undifferentiated and has a chondritic signature ($\epsilon_{182W}=0$). Upon collision, the impactor is assumed to differentiate. Had it not merged, the subsequent evolution of its tungsten anomaly is shown by the dashed line — a lower ϵ_{182W} results because of the later differentiation. Because it does in fact merge with the target, the tungsten anomaly of the resulting object is reduced relative to the target's value. In Fig. 1b both objects are differentiated, and evolve towards positive ϵ_{182W}. However, because the collision involves the impactor's core re-equilibrating with the silicates, the overall tungsten anomaly is greatly reduced relative to the pre-impact values. Finally, in Fig. 1c both objects are again differentiated, but this time the cores and mantles merge without any re-equilibration. The resulting mantle ϵ_{182W} is accordingly a weighted mean of the target and impactor values.

At this point, it may be helpful to itemize the factors which control the present-day value of ϵ_{182W} observed.

1. Timing of impacts. A differentiation event which occurs early is likely to have a larger isotopic signature, because more ^{182}Hf is available to decay into ^{182}W. For the same reason, an early impact which causes re-equilibration will cause a smaller reduction in the final isotopic anomaly than a later impact.
2. Partitioning behaviour (D, $f^{Hf/W}$). If W partitions more strongly into the core during differentiation, a stronger (mantle) tungsten anomaly will result, as will a higher value of $f^{Hf/W}$. This latter value is difficult to measure directly, since it can be reset by other processes such as crustal extraction ([22], e.g). However, it can be inferred from other elemental ratios such as W/Th ([53], e.g.).
3. Relative masses of colliding objects. The absolute masses of the colliding objects are not important, but their relative masses are: a relatively small impactor will have a smaller effect on the overall isotopic signal, other things being equal. The relative masses will also influence the equilibration style (see Section 2).
4. Silicate mass fraction (y). A smaller mantle relative to the core will result in an increased Hf concentration during differentiation (Eq. (3)) and thus an increased tungsten anomaly.
5. Style of re-equilibration during collisions. As discussed above (Section 2)), the degree to which re-equilibration occurs during a collision can have a significant effect on the isotopic outcome (see Fig. 1).
6. Initial state of colliding bodies. As discussed above, whether or not the colliding bodies are already differentiated can affect the resulting isotopic signature (see Fig. 1).

It should be clear from this list that there are many potential tradeoffs. For instance, an early impact with "mantle equilibration" and a later impact resulting in core merging can produce the same tungsten anomaly. The advantage of using N-body simulations is that the timing of the impacts (factor 1) and the relative masses (factor 3) are not free parameters, and we can therefore investigate the effects of some of the other factors. In this work we focus on factors 4–6; variable partition coefficients (factor 2) are not addressed in detail, but may have significant effects and should be the focus of future work.

In order to check the code, we discretized the exponential growth curve of [52] into 100 equally sized impacts, and verified that our results agreed with those

in Fig. 7 of [52] for both the mantle equilibration and primitive differentiation cases. We also tracked the evolution of single objects following differentiation to ensure that they reproduced Eq. (12) of [5]. The timestep used in calculating isotopic evolution was the smaller of 0.25 Myr and 10% of the time interval between successive impacts.

3.1. Model parameters

Following [5], we assumed initial concentrations relative to ^{183}W for ^{182}Hf, ^{182}W and ^{180}Hf of 2.836×10^{-4}, 1.850664 and 2.836, respectively. In most cases we assumed a constant silicate mass fraction $y=0.68$ to reflect that of the Earth. Based on inferred fractionation factors for the mantle and core of 12 and −1, respectively (see [5]), the partition coefficients were set to $D^{\mathrm{Hf}}=10^4$ and $D^{\mathrm{W}}=0.0392$. Generally, all bodies were assumed to start undifferentiated. As discussed above, for the Moon- to Mars-sized starting bodies modelled, it is not clear that this assumption is correct. We discuss the effects of early differentiation further below (Section 4.1).

As described in [1], the dynamical evolution simulations were initiated using the output from an accretion model by [12]. This model generated a roughly constant mass distribution (total 1.77 M_e) between 0.5 and 1.5 AU, distributed among 22 planetesimals with median, maximum and minimum masses of 0.085, 0.144 and 0.013 M_e, respectively. We used the results from 5 separate simulations (numbers 3 and 5–8 from [1]), which resulted in 4–7 final bodies of mass up to ≈1 M_e. The median collision time and post-collision body mass were 3.8 Myr and 0.27 M_e, respectively.

As discussed above and in [45], it is possible that the largest impacts (for instance, the one which led to the formation of the Moon) may have isotopic effects distinct from smaller events. The critical size is not clear, but is probably comparable to the size of the Earth prior to the Moon-forming impact (roughly 0.9 M_e [43]). Here we (arbitrarily) define a "giant" impact as one which involves at least one body in excess of 0.5 M_e, and an impactor : target mass ratio ≥ 0.1. Only 8% (seven) of all the collisions fall into this category; the mean time of these impacts is late (30 Myr) and the mean resulting mass is large (0.7 M_e).

3.2. Observations

The isotopic observational constraints we will use are explained in detail in [5] and are reproduced here in Table 1. The physical constraints are reproduced from [54]. Two sets of values are given for Mars, because that body appears to have (at least) two isotopically distinct reservoirs: one from the Shergottite meteorites (S); the other from the Nakhlites and Chassignites (NC). The Martian values obtained by [22] are slightly different to those employed here. Interpretation of the NC results is complicated by Hf–W fractionation as a result of early crust–mantle differentiation [55]. Although we focus on the nominal Mars NC values, because these place an apparently stronger constraint on the end of accretion, both S and NC values are plotted to facilitate comparison with the model results.

Table 1
Characteristics of present-day inner solar system bodies, from [5] and [54]

Body	M (M_e)	a (AU)	ϵ_{182W}	$f^{Hf/W}$	y
Mercury	0.055	0.387	–	–	0.3
Venus	0.816	0.723	–	–	0.7
Earth	1	1	1.9±0.2	12±2	0.675
Moon	0.012	–	3.2±0.4	15±2	0.98
Mars S	0.108	1.524	2.4±0.5	2±0.8	0.8
Mars NC	0.108	1.524	4.4±0.5	6±1	0.8
Vesta	5×10^{-5}	2.36	19±2	15±2	0.8

M is mass, M_e is the mass of the Earth, a is semi-major axis.

The tungsten anomaly value for the Moon is uncertain owing to cosmic ray production of ^{182}W [56]. In the following discussion, we generally neglect the Moon, because it formed from debris spalled off during a giant impact [43]. Since the accretion models of [1] cannot explicitly treat such processes, these models cannot be compared directly with lunar observations. We do, however, briefly consider the consequences of likely "Moon-forming" impacts in Section 4.4.

4. Results

Fig. 2a shows the growth curves of the particles in a typical N-body simulation, where each curve is truncated when the object collides with a bigger one. In this case, the bulk of accretion is complete in ≈50 Myr and results in four bodies (A–D). Most of the collisions occur early and between bodies which are relatively small, but there are two late collisions which qualify as "giant" (as defined above). Particles A,B,C and D exceed 63% of their final mass at 28, 23, 84 and 16 Myr, respectively. In a simple exponential model of growth, such mean growth times can be used to predict the resulting ϵ_{182W} [45], with earlier times leading to larger isotopic anomalies.

Fig. 2b and c demonstrates the ϵ_{182W} evolution of these bodies under different equilibration assumptions.

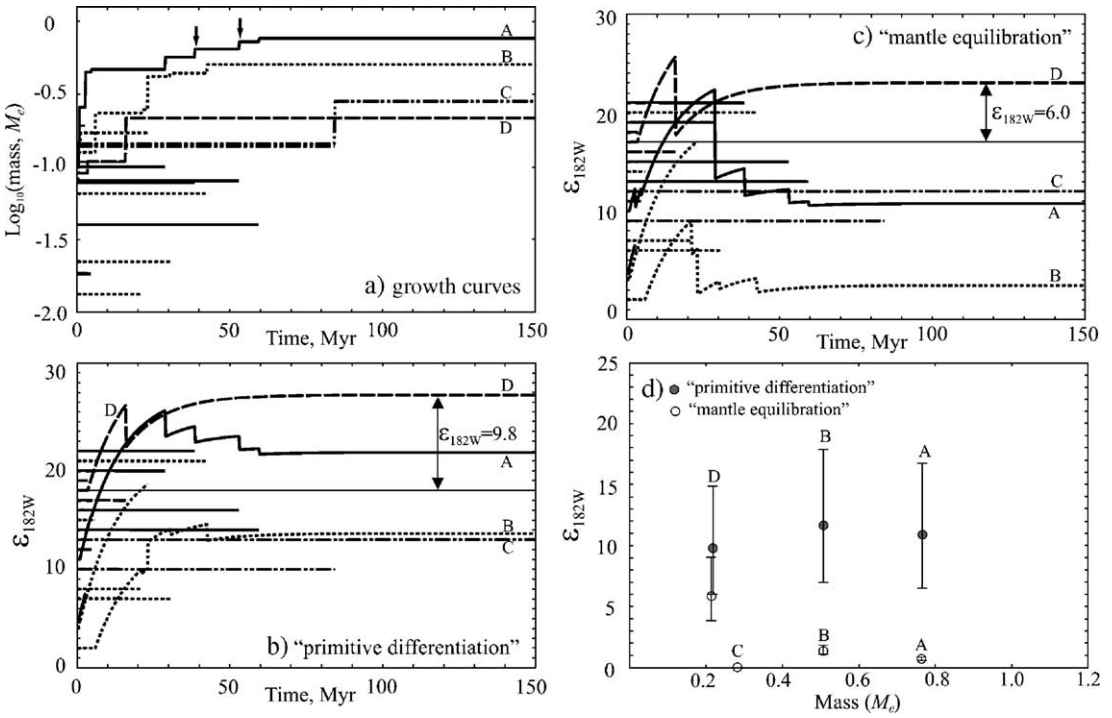

Fig. 2. a) Growth curves of particles in N-body simulation (run 5 from [1]), plotting log10 mass (M) in units of one Earth mass (M_e) against time. Curves are truncated when particle merges with larger particle. A–D refer to bodies surviving at the end of the simulation. Individual curves have different line styles according to which final body each particle accretes to. Arrows denote "giant" impacts, as defined in the text. b) Evolution of ϵ_{182W} for individual particles, assuming primitive differentiation. Values for successive particles are offset by one ϵ-unit for clarity; particle D shows an example of how to read the ϵ_{182W} value. Here $y=0.68$ and $f^{Hf/W}=12$ for all particles. c) As for b), but assuming "mantle equilibration". d) Summary of results from b) and c), plotting final particle mass M against ϵ_{182W} for two different re-equilibration scenarios. Range of values obtained by varying y from 0.78 (low ϵ_{182W}) to 0.58 (high ϵ_{182W}).

In Fig. 2b, primitive differentiation is assumed to operate. For example, particle A suffers an early impact, causing it to differentiate and the mantle ϵ_{182W} to grow until a later collision with a previously undifferentiated object at 28 Myr. This and later collisions dilute the original isotopic signal; particle D undergoes a similar evolution but with fewer collisions. Particle C illustrates the fact that a late (84 Myr) collision has no effect on the isotopic signature, because all the ^{182}Hf has already decayed. Finally, particle B shows an increase in ϵ_{182W} during a collision at 23 Myr because the impactor differentiated early and thus has a high ϵ_{182W}, which is added to the target's mantle without equilibration. This example illustrates the importance of tracking the isotopic evolution of all particles, rather than simply following the growth of one body.

Fig. 2c shows the results assuming mantle equilibration. Here, once differentiation has occurred, all subsequent impacts result in a reduction in ϵ_{182W} because the impactor's core re-equilibrates with the mantle material and thus reduces the radiogenic tungsten excess.

Fig. 2d summarizes the final ϵ_{182W} values for each of the two equilibration scenarios. As expected, the mantle equilibration scenario results in lower values than the primitive differentiation scenario. The error bars for each point result from varying the silicate mass fraction y between 0.58 (higher ϵ_{182W}) and 0.78 (lower ϵ_{182W}). The magnitude of the effect is quite large, and suggests that small variations in y can lead to large variations in ϵ_{182W}. This is an issue we return to below (Section 4.3).

Fig. 3 summarizes results from all 5 N-body simulations, and Table 2 tabulates these results. Fig. 3a plots the final mass M against semi-major axis a, and compares the results with the observed terrestrial planets and Vesta. As discussed in [1], it is clear that the accretion simulations do a reasonable job of generating terrestrial planetary systems like our own. However, the model eccentricities are higher than those observed [[2], c.f.], likely because the models did not incorporate interactions with either a remnant disk of gas [57,58] or small planetesimals [59].

Fig. 3b and c plots ϵ_{182W} against M for the mantle equilibration and primitive differentiation scenarios,

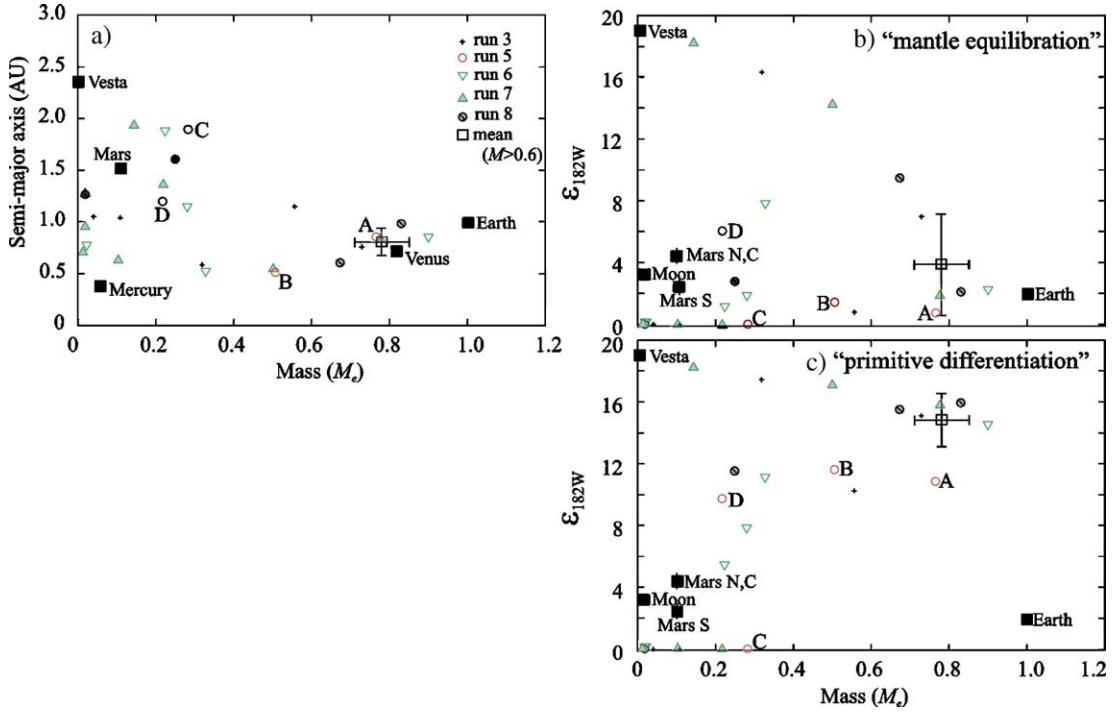

Fig. 3. a) Final outcomes of 5 N-body simulations (Table 2), plotted in mass-semimajor axis space and compared with terrestrial planet values (Table 1). Open square with error bars gives mean and standard deviation of model mass and semi-major axis for bodies with $M \geq 0.6\ M_e$. Letters A–D refer to particles shown in Fig. 2 and discussed in the text. b) Corresponding ϵ_{182W} values, assuming mantle equilibration. c) As for b), but assuming primitive-differentiation.

respectively. For the mantle equilibration scenario, there is a clear trend of decreasing ϵ_{182W} as M increases. This is to be expected, because larger bodies typically suffer more collisions, and Fig. 2c demonstrated that collisions lead to a reduction in ϵ_{182W}. Conversely, the primitive differentiation scenario leads to high ϵ_{182W} even for large M. This is because the initial differentiation signature is less affected by later impacts if merging, rather than re-equilibration, occurs.

An important aspect of Fig. 3b and c is that the isotopic variability between larger bodies is significantly less than that between smaller bodies. For both Fig. 3b and c, the standard deviation of the ϵ_{182W} values of small bodies ($0.05 \leq M/M_e \leq 0.3$) is roughly twice that of larger bodies ($M/M_e \geq 0.6$). This effect is a result of the averaging effect of impacts, which is more important for bodies which have suffered more impacts and are thus larger.

Fig. 3b and c also plots the observed planetary masses and mantle ϵ_{182W} values (Table 1). Despite the paucity of data points, and the stochastic nature of the accretion process, it is clear that Fig. 3b (mantle equilibration) provides a better fit to the observations than does Fig. 3c (primitive differentiation). The mean mass and ϵ_{182W} obtained for model bodies with $M/M_e \geq 0.6$ (open squares) show that under the primitive differentiation scenario, bodies approaching the mass of the Earth result in values of ϵ_{182W} which are much higher than the observed value.

If primitive differentiation/core merging were in fact a better representation of reality, then to generate Earth-like isotopic results either the timescale for accretion would have to be extended, or the fractionation of W into the core reduced. The former is not plausible: even artificially expanding the accretion timescale by a factor of 5 results in a mean ϵ_{182W} for $M/M_e \geq 0.6$ of 10 ± 2, still in excess of the terrestrial value. Increasing D^W by a factor of three results in an Earth-like ϵ_{182W} value, but results in an $f^{Hf/W}$ value of 4, inconsistent with the observed value of 12 ± 2. It is possible that a time-varying W partition coefficient (as proposed by [4]) might allow a primitive differentiation scenario compatible with the constraints. However, the simplest conclusion is that the mantle equilibration scenario is most consistent with the observations.

This conclusion is significant: it suggests that even late-stage, large impacts result in re-equilibration of the impacting body (Fig. 1b), rather than core merging (Fig. 1c). Similar conclusions have previously been reached by [3,5] regarding the Earth–Moon impact and [22] regarding Earth and Mars. The occurrence of re-equilibration

Table 2
Results of isotopic calculations for final bodies generated by N-body calculations [1]

Run	M (M_e)	a (AU)	ϵ_{182W}	ϵ_{182W}	y	$f^{Hf/W}$	ϵ_{107Ag}
3	0.32	0.57	16.3	34.5	0.50	25.5	−0.80
	0.56	1.18	0.8	0.9	0.75	9.2	−0.03
	0.73	0.73	7.0	4.6	0.72	7.6	−0.25
5B	0.51	0.53	1.4	1.6	0.59	15.0	−0.01
A	0.77	0.87	0.7	0.7	0.66	8.9	−0.01
C	0.28	1.78	0.02	0.	0.80	6.4	0.
D	0.22	1.30	6.0	3.6	0.79	6.6	−0.21
6G	0.90	0.81	2.1	2.3	0.72	13.5	−0.04
	0.33	0.51	7.7	11.8	0.63	19.7	−0.25
	0.28	1.14	1.7	1.8	0.67	8.8	−0.03
	0.22	1.86	1.0	1.0	0.73	7.5	−0.03
7	0.50	0.57	14.2	29.6	0.50	25.5	−0.64
	0.78	0.82	1.9	1.5	0.77	8.0	−0.05
	0.22	1.36	0.	0.	0.80	6.4	0.
F	0.14	1.94	18.2	16.6	0.70	10.9	−0.94
8	0.67	0.61	9.5	9.7	0.58	11.9	−0.33
	0.83	0.98	2.1	1.9	0.77	8.3	−0.06
	0.25	1.66	2.8	2.3	0.77	8.9	−0.17

Only bodies which suffered one or more collision are tabulated. The first ϵ_{182W} value is calculated using the mantle equilibration scenario with constant y (Fig. 3b); the second value assumes an initially radially vari-able y, also tabulated (Fig. 5). The final column calculates ϵ_{107Ag}, using the same form as Eq. (8) and referenced to ^{109}Ag; these calculations also assume ra-dially variable y and use partition coefficients and initial ratios given in the text. These values are negative because Pd partitions more strongly into the core than Ag. A–G refers to individual bodies discussed in the text.

during large impacts in turn places constraints on the likely microphysics operating during such events. We discuss these issues further below (Section 5).

4.1. Early core formation

Having considered the outcomes based on two end-member re-equilibration scenarios, we now consider the effect of three complications. The first complication is that, as noted above, some or all of the planetesimals may have differentiated prior to the first impact occurring in the N- body simulations. Accordingly, we carried out calculations identical to those shown in Fig. 3b and c, except that all undifferentiated planetesimals were assumed to differentiate at 3 Myr, based on timescales from Vesta and the iron meteorites (Section 2). In the case of the primitive differentiation scenario (not shown), the results are high ($\epsilon_{182W} \approx 16$) and relatively uniform isotopic anomalies. This effect is identical to that found by [3,4] and arises because differentiated objects merge without any re-equilibration, and thus retain the isotopic signal of the original core differentiation event.

Fig. 4a plots the isotopic evolution of the same embryos shown in Fig. 3a, but now assuming early core formation and mantle equilibration. The isotopic growth following core formation is clearly visible. However, most bodies suffer subsequent impacts which lead to isotopic re-equilibration and thus a reduction in ϵ_{182W}. A particularly striking example is particle C, which undergoes a late collision at 84 Myr with an almost identical mass object. The result is a large reduction in ϵ_{182W}.

The main effect of early core formation, therefore, is to generate large values of ϵ_{182W} in bodies which do not suffer subsequent impacts and re-equilibration. This is shown in Fig. 4b, which plots ϵ_{182W} against mass M. Here the solid vertical lines show changes from the results without early core formation (Fig. 3b). As expected, large bodies show no change, while most small bodies show elevated values of ϵ_{182W}.

This result presents a potential problem for Mars. On the basis of accretion simulations, it has been suggested [15] that Mars is a "stranded embryo" which formed rapidly by runaway growth (within the first ≈1 Myr). Such a scenario suggests a high fraction of the total planet mass being delivered in small bodies, with few late, large impacts. If core formation occurred during this early accretion, Fig. 4b suggests that the resulting value of ϵ_{182W} might be higher than that observed. However, the values of y and $f^{Hf/W}$ for Mars are significantly different to those for Earth (Table 1), which affects the isotopic anomalies generated.

Fig. 4c therefore plots the same evolution as in Fig. 4a, but using Mars-like values of y (0.8) and $f^{Hf/W}$ (3.2). Because of the parameters adopted, the isotopic anomalies generated are smaller than in Fig. 4a. Fig. 4d summarizes the results obtained and shows that early (3 Myr) differentiation is consistent with the Martian parameters adopted. Earlier (1 Myr) differentiation leads to only minor (≈0.4 ϵ units) increases in the mean tungsten anomaly for Mars-mass (<0.15 M_e) objects. There is thus no obvious conflict with the idea of Mars as a stranded embryo. However, this model, unlike that shown in Fig. 4b, fails to produce any Vesta-like isotopic signatures, because of the values of $f^{Hf/W}$ and y adopted. As we will demonstrate below, allowing y to vary radially results in models which can generate Earth-, Mars- and Vesta-like results simultaneously. Furthermore, we also demonstrate that giant impacts on Mars subsequent to its runaway growth are dynamically plausible and do not violate the isotopic constraints.

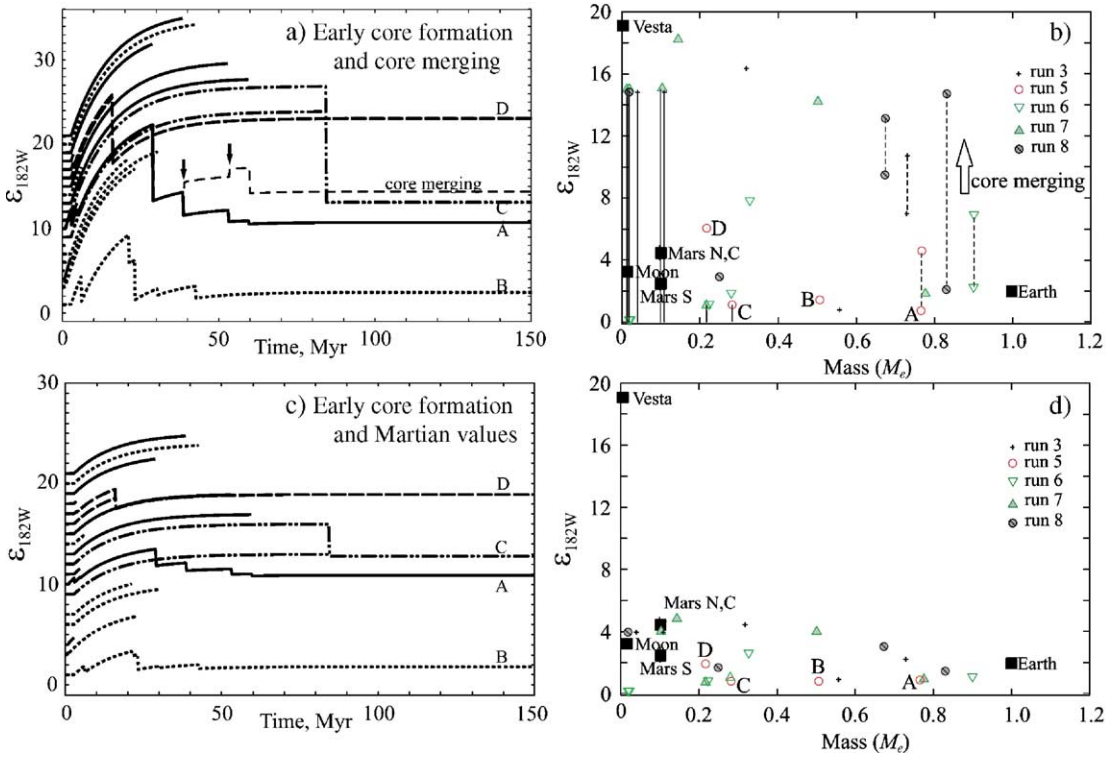

Fig. 4. a) As for Fig. 2c (mantle equilibration), but assuming that any previously undifferentiated object differentiates at 3 Myr. Thin dashed line shows isotopic evolution of particle A if giant impacts (marked with arrows) lead to cores and mantles merging without equilibration. A giant impact is one in which at least one body exceeds $0.5M_e$ and the mass ratio exceeds 0.1. b) Summary of results from all 5 runs assuming early core formation and mantle equilibration. Vertical solid lines indicate change in outcomes compared with Fig. 3b. Points connected by vertical dashed lines show outcomes depending on whether giant impacts do (higher values) or do not (lower values) lead to merging without equilibration. c) As for Fig. 4a, but using values of y (0.8) and $f^{Hf/W}$ (3.2) appropriate to Mars. d) As for Fig. 4b, but with Martian values (change in outcomes from Fig. 3b are not plotted).

4.2. Effects of largest and smallest impacts

Our calculations generally assume that any impact results in core formation for objects not already differentiated. For the smallest objects ($<\sim 0.1\ M_e$) it is not clear that this assumption is warranted. Accordingly, we repeated the calculations shown in Fig. 3b but only allowed differentiation to occur if one of the colliding objects exceeded 0.1 M_e. The results (not shown) were almost identical to Fig. 3b, except that a few more small objects never underwent differentiation and thus retained chondritic signatures ($\epsilon_{182W}=0$).

More significant is the potential effect of giant impacts. As discussed above, it is possible that giant impacts lead to merging of cores and mantles without any isotopic equilibration. Fig. 4a also shows (thin dashed line) an example isotope evolution plot for particle A in the case when the two largest collisions (arrows) lead to core merging. Unlike the standard case (bold line), in which these two collisions reduce the tungsten anomaly, here the collisions actually increase the anomaly slightly, because in each case the impactor has a high ϵ_{182W} value as a result of early core formation. Fig. 4b shows that if large impacts lead to direct core mergers, the mean tungsten anomaly for bodies with $M/M_e \geq 0.6$ increases from 4 to 8.5, significantly in excess of the value for Earth. The "giant impact merger" scenario is therefore problematic: it predicts ϵ_{182W} values for Earth-sized objects which are too large. As before, this result strongly suggests that even the largest impacts do not result in core merging, but instead that the impactor at least partially re-equilibrates with the target's mantle material.

4.3. Effects of spatial heterogeneity

Finally, we relax our assumption that the initial planetesimal population was compositionally homogeneous. There are several lines of evidence against this simplifying assumption (see also the discussion of heterogeneous accretion in [45]). Firstly, values of $f^{Hf/W}$ vary quite widely between different bodies (Section 3.2),

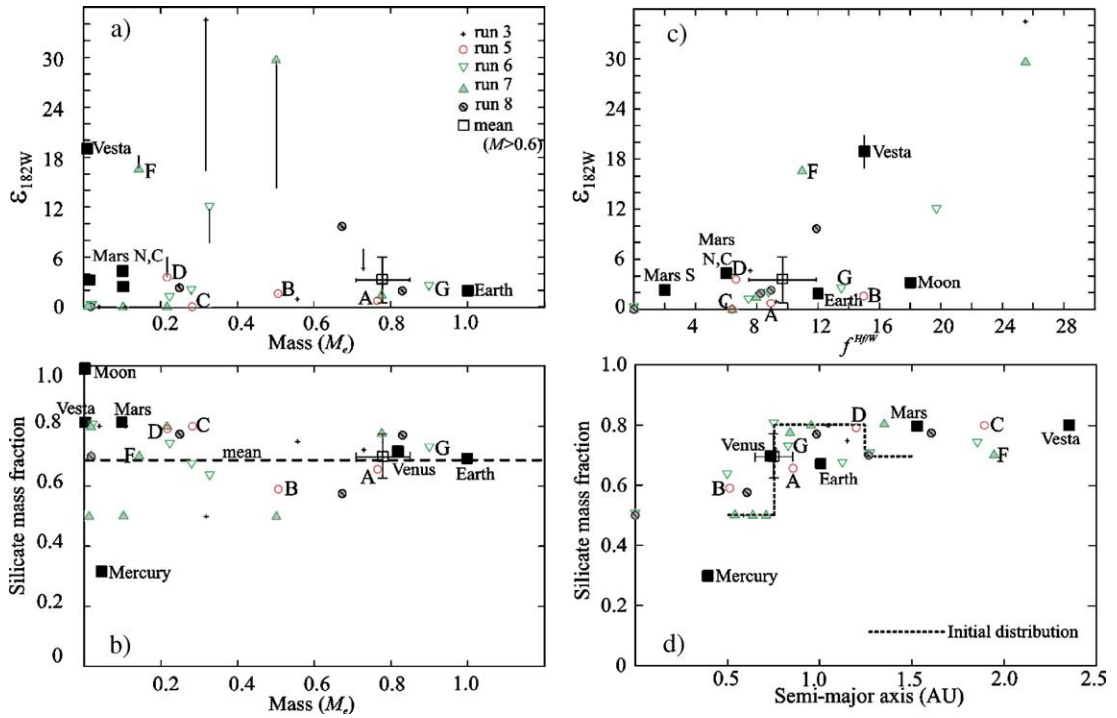

Fig. 5. a) As for Fig. 3b (mantle equilibration), but assuming a spatially varying silicate mass fraction (y) in the original planetary embryos. Dotted line in d) denotes the initial variation in y. The open box and error bars denote model mean and standard deviation for bodies with $M \geq 0.6\ M_e$. Particles A–G are discussed in the text. b) Final value of y versus final body mass. c) Tungsten anomaly versus mantle Hf/W ratio. d) Silicate mass fraction versus semi-major axis.

suggesting some combination of variations in partition coefficients D or silicate mass fraction. Secondly, the observed core : silicate ratio within the terrestrial planets varies quite widely (Table 1). Some of this variation may be due to the stripping of planetary mantles by late-stage impacts (a process not modelled in our N-body simulations, but which may have been important for Mercury [60]). However, it is also possible that planetesimals which formed close to the Sun developed higher iron : silicate ratios [61], and were depleted in volatiles, leading to potential variations in oxygen fugacity and D. Further evidence for this effect comes from the correlation of Rb/Sr with Hf/W, which suggests a link between volatile abundance and partitioning behaviour [4]. Thirdly, experimental work suggests that D is likely to vary as a function of pressure and temperature as well as oxygen fugacity [51], and is thus unlikely to be constant as planetesimals evolve and grow. Finally, other isotopic systems suggest that compositional gradients may have been present during accretion. For instance, although Sr [32] and W [22] isotope ratios appear to have been relatively homogeneous in the early system, there is evidence for radial variations in Cr isotope ratios [32], based on terrestrial, Martian and meteorite samples.

Clearly, relaxing the assumption of radial homogeneity opens up a very broad parameter space, with some of the parameters (e.g. likely temporal and spatial variations in D) being very poorly constrained. We do not propose to carry out a full parameter space exploration here; instead, we focus on variations in a single parameter (the silicate mass fraction y). The main reason for focusing on this parameter is that theoretical expectations suggest, and observations confirm, that the silicate mass fraction of planets does indeed vary; and that modelling the effect of variations in y is relatively straightforward. Although we conclude that moderate variations in y can successfully reproduce the observed isotopic and physical variability of the terrestrial planets, we cannot rule out other mechanisms. For instance, it is quite likely that the tungsten partition coefficient varied in both space and time, and there may also have been variability in the initial Hf/W ratios of the planetesimals.

Variations in y are expected, for reasons outlined above, and can have dramatic effects on the isotopic signals (Fig. 2d). To illustrate these effects, we imposed an initial radial heterogeneity in y as follows: embryos with initial semi-major axes in the range 0.5–0.75, 0.75–1.0, 1.0–1.25 and 1.25– 1.5 AU were

assigned y values of 0.5, 0.8, 0.8 and 0.7, respectively. This distribution approximates the expected silicate depletion close to the Sun, and results in the same mass-weighted value of y (0.68) as in our previous calculations. Fig. 5d shows the initial distribution assumed, and the final results. There has clearly been a considerable degree of mixing between bodies from different initial semi-major axes ([62–64], c.f.), but the initial trend of higher iron fractions towards the Sun has not been entirely removed.

Fig. 5a plots the results (tabulated in Table 2), assuming mantle equilibration, in M–ϵ_{182W} space. The vertical lines show the change in values compared with the (constant y) results plotted in Fig. 3b. In some cases, the changes are dramatic. These changes can be understood by inspection of Fig 5b, in which the final silicate mass fraction of each body y is plotted as a function of M. Bodies with a value of y lower than the mean value tend to show an increase in ϵ_{182W} as expected, and vice versa. Larger bodies typically show smaller changes simply because their silicate mass fractions are closer to the mean value, as a result of more collisions having occurred. This averaging is also reflected in the reduction in isotopic variability for larger bodies: again, large bodies ($M \geq 0.6\ M_e$) show an isotopic standard deviation about half that of smaller ($0.05 \leq M/M_e \leq 0.3$) bodies.

The observed variation in $f^{Hf/W}$ between solar system bodies may arise because of variations in either y, D or (most likely) some combination of the two. As noted above, here we generate variations in $f^{Hf/W}$ by varying y only. Fig. 5c plots ϵ_{182W} against $f^{Hf/W}$ and shows a rough correlation, as expected: more hafnium-rich mantles generally result in mantles with larger tungsten anomalies. This plot also shows that similar values of ϵ_{182W} can arise from quite different values of $f^{Hf/W}$, depending on the impact history. Fig. 5 demonstrates that relatively modest spatial variations in y generate variations in both ϵ_{182W} and $f^{Hf/W}$ similar to those observed (see below). This is in contrast to Fig. 4b and d, which showed a more restricted range in ϵ_{182W} when using the same impact histories but a constant value of y.

In reality, parameters other than y are also likely to be variable. For instance, a radial variation in D^W of a factor of 4 (0.018–0.073) will have the same effect as the radial variation in y shown in Fig. 5d. As argued above, D^W is also likely to vary in time and depend on the thermal evolution of each planetesimal. We have neglected these effects here not because they are unimportant, but because it is unclear how to go about modelling them.

4.4. Comparisons with observations

In general, Fig. 5 suggests that the numerical simulations, assuming mantle equilibration and initial spatial heterogeneity in y, can generate planetary characteristics similar to those actually observed. For instance, the mean y, ϵ_{182W} and $f^{Hf/W}$ values for the large model bodies are all within one standard deviation of the Earth's values. Bodies with isotopic characteristics similar to Mars and Vesta are also produced, though here direct comparisons are hampered because of the large starting masses of the model particles. Despite the simplifications adopted, notably the constant value of D^W, the degree of agreement between the numerical results and the observations is encouraging.

Because of the stochastic nature of late-stage giant impacts, and the limited number of simulation results used here, focusing on the histories of individual particles can only provide plausible examples of isotopic evolution. The conclusions presented below are therefore preliminary, and their robustness will need to be verified by running much larger numbers of simulations and examining the role of different initial size-distributions of planetesimals.

An "Earth-like" result is generated by particle G (Table 2). This particle has values of ϵ_{182W}, $f^{Hf/W}$, M and a all within 20% of the observed values (Table 1). The growth history of this particle is shown in Fig 6a: the last large impact, responsible for 35% of its final mass, occurs at 28.5 Myr. The impacting body in this case is differentiated, with $\epsilon_{182W} = 10$ prior to impact, because of its own collision history (see Fig. 6b). As noted above, if this final impact simply caused a core merging event, rather than isotopic re-equilibration, the resulting tungsten anomaly would be too large (see Fig. 4b). While this result argues against the occurrence of simple core merging during even Moon-forming impacts, it is a single model outcome involving highly stochastic processes. Further study, investigating the results of multiple model outcomes, is clearly required.

Another interesting aspect of particle G's history is that the large impact at 28.5 Myr represents enough mass and angular momentum to qualify as a potential "Moon-forming impact" [1]. Although the N-body code does not include the fragmentation and re-accretion processes responsible for the Moon's formation, the isotopic history of a body re-accreting as a result of an impact can be calculated using Eq. (12) of [5]. Fig. 6b shows such a history (dashed line) for an object formed at 28.5 Myr with an initially chondritic composition and $f^{Hf/W} = 18$ (note that other assumptions regarding $f^{Hf/W}$ and the initial isotopic composition can lead to quite

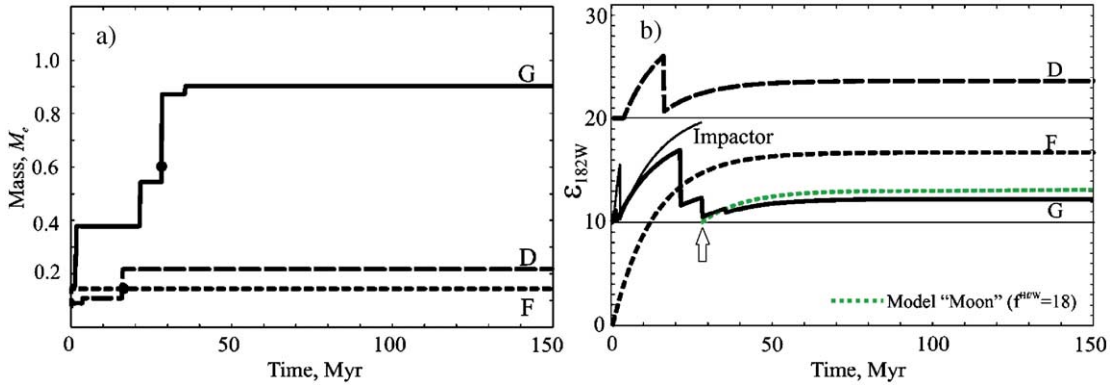

Fig. 6. a) Growth curve of three bodies discussed in more detail in the text. Black dots denote the time at which each body exceeds 63% of its final mass. b) Isotopic evolution curves for same bodies, assuming mantle equilibration and spatially variable y (Fig. 5). Successive offsets of 10 ϵ-units have been applied to F, G and D. For body G, the evolution of a Moon-like body due to an impact is calculated by assuming a core separation time of 28.5 Myr (arrow), an initially chondritic composition, $f^{Hf/W}=18$ and using Eq. (12) of [5]. Thin solid line gives the isotopic evolution of the body responsible for this impact, showing its pre-impact $\epsilon_{182W}=10$ (see text).

different results — a more thorough discussion of these issues may be found in [4] and [3]). The final tungsten anomaly obtained ($\epsilon_{182W}=3$) is indistinguishable from that observed on the Moon. Thus, particle G represents a model outcome which could have generated a system isotopically and physically resembling the Earth–Moon system.

One problem with relating this specific model to the Moon is that the isotopic results require the impactor mantle and core to re-equilibrate with the target mantle. Because of the large tungsten anomaly of the impactor ($\epsilon_{182W}=10$), mantle material not re-equilibrating (for instance, material flung off into the proto-lunar disk) would have a tungsten anomaly much larger than the observed lunar value. On the other hand, mantle material which did re-equilibrate (as is also suggested by the identical oxygen isotope characteristics of the Earth and Moon [65]), would likely attain an iron concentration higher than is observed for the Moon ([43], e.g.). One possible resolution is simply that the body which impacted the Earth had an initial tungsten anomaly much lower than the impactor considered here; further study of this issue is warranted.

Particle D results in very Mars NC-like values of ϵ_{182W}, $f^{Hf/W}$ and silicate mass fraction (Table 2). The final mass is too large and the semi-major axis is 15% too small. The first effect arises because of the large masses of the initial planetesimals; simply reducing the masses of all the initial planetesimals by a factor of 2 would have no effect on the isotopic outcome if the collisional history were otherwise unchanged. The extent to which the dynamics would in fact change is unclear and should be addressed in future work using larger numbers of smaller initial particles.

The history of this object is also shown in Fig. 6. The last important collision in this model occurs at 16 Myr. If exponentially decaying planetary growth were assumed, the model values of ϵ_{182W} and $f^{Hf/W}$ would result in a mean time to form 63% of the final mass $\langle t\rangle$ of about 5 Myr, significantly shorter than the timing of the final impact. Jacobsen [5] similarly finds that realistic growth models result in final giant impacts significantly later than the mean growth time. This factor of three discrepancy illustrate the shortcomings of inferring accretion histories based on simple analytical assumptions of planetary growth.

The isotopic results for Mars suggest that re-equilibration during collisions was an important factor. Such re-equilibration could occur either because Mars possessed an early magma ocean [22], or because the accretion of Mars mainly involved impactors much smaller than the target. Whether or not Mars possessed an ancient magma ocean is currently unclear (see discussion in [66]).

The large reduction in particle D's tungsten isotopic anomaly at 16 Myr occurs because the colliding objects have similar masses and there is relatively little live ^{182}Hf remaining. An identical impactor occurring later would result in an even larger reduction in tungsten anomaly. A smaller impactor, such as the putative cause of the Martian hemispheric dichotomy [67], would have a negligible effect on the isotopic signature because of its small mass (~1% of the target). The isotopic effects of the last bodies to impact Mars therefore depend on a combination of both size and timing; such effects cannot be modelled using simple analytical assumptions of planetary growth.

Although a Mars which completed its formation after 1–3 Myr is compatible with the isotopic evidence (Section 4.1), the history of particle D demonstrates that a more prolonged history, involving late, large impacts which re-equilibrate with the mantle, is dynamically plausible and equally compatible with the isotopic observations. Thus, suggestions that Mars is a stranded planetary embryo left over from the early (~1 Myr; [12], e.g.) runaway growth phase of accretion [15] are consistent with, but are not required by, the isotopic observations.

Finally, particle F has the closest isotopic resemblance to Vesta, in particular its extreme value of ϵ_{182W}. This "model Vesta" is much larger than the real object, owing to the limitations on the starting particle masses, but its dynamical and isotopic behaviour provide a good example of how the real Vesta may have evolved. The reason for the high ϵ_{182W} is evident from Fig. 6: the last collision which involved this particle occurred at 0.12 Myr, allowing differentiation while large amounts of radiogenic ^{182}Hf were present. Subsequent collisions did not occur, mainly due to the particle's large semi-major axis and consequent isolation from other bodies. Although our model assumes differentiation occurs as a result of impact, in reality Vesta may have instead undergone early differentiation due to the presence of live ^{26}Al [30]. In either case, the main result is that it is dynamically possible for a small body to be isolated since very early in the history of the Solar System, and thus to undergo radiogenic ingrowth without the isotopic anomalies being re-set by later collisions.

4.5. Predictions

An advantage of the approach presented here is that it can be applied to any suitable isotopic system. As an example, the final column in Table 2 gives the ^{107}Ag isotopic anomaly predicted by the y-variable model. The Pd–Ag system is similar to the Hf–W system but has a shorter half-life (6.5 Myr).

To carry out these calculations, we assumed initial concentrations of ^{107}Pd, ^{107}Ag and ^{108}Pd relative to ^{109}Ag of 1.106383×10^{-4}, 1.0851 and 4.617, respectively, based on the results of [17] and the compilation in [54]. We also used the latter to infer partition coefficients $D^{Pd}=1.6\times10^{-3}$ and $D^{Ag}=0.028$. The resulting mantle values of ϵ_{107Ag} (defined in a manner analogous to Eq. (8)) are negative because Pd partitions more strongly than Ag into the core. We caution that the initial concentrations assumed are based on measurements that are technically very challenging [68], and may need to be revised in future.

As one would expect, there is a rough correlation between tungsten and silver isotopic anomalies (Table 2). The amplitude of the silver anomalies, however, is subdued, because the shorter half-life means that only early differentiation events generate strong signals, and the difference in partitioning is less extreme than for the Hf–W system. The silver anomaly of the Earth-like body (particle G) is close to chondritic ($\epsilon_{107Ag}\approx0$), because of its slow accretion relative to the half-life of 6.5 Myr. Thus, if the Earth possesses a chondritic Ag isotopic signature, this observation places a lower bound on the Earth's accretion timescale. On the other hand, the Vesta-like body (particle F) shows a strong signal ($\epsilon_{107Ag}=-0.94$) because of its early differentiation and subsequent isolation. The Mars-like body (particle D) has a subdued signal ($\epsilon_{107Ag}=-0.21$). More rapid accretion would result in a stronger signal: for instance, artificially reducing the accretion timescale by a factor of 3 results in an $\epsilon_{107Ag}=-0.56$. Thus, future measurements of the Pd–Ag isotopic system, although technically challenging, are likely to throw further light onto the timescale of accretion.

5. Conclusions and further work

In this work, we have performed isotopic calculations based on dynamical N-body simulations of terrestrial planet accretion. The main conclusion is that, under certain circumstances, the results can reproduce the observed physical (M, a) and isotopic (ϵ_{182W}, $f^{Hf/W}$) characteristics of the inner solar system (e.g. Fig. 5). In particular:

1) The isotopic variability recorded in smaller objects is greater than that in larger objects, simply because larger objects suffer more collisions, which drives the isotopic signatures towards an average value.
2) The best match to the observations is obtained when even the largest impacting bodies re-equilibrate with the target's mantle, rather than undergoing direct core merging. This conclusion is in agreement with arguments by [5],
3) Observed variations in $f^{Hf/W}$ can be explained by an initial radial variation in planetesimal silicate mass fraction y (though in reality, both spatial and temporal variations in D are also likely to play a role — see below).
4) Late (~10 Myr) giant impacts, a common feature of our dynamical models, are consistent with Martian isotopic observations, and suggest that Mars may not simply be a stranded planetary embryo.It should be

clear that the analysis presented here is limited in several important respects. Firstly, the minimum initial body mass modelled is not much less than that of Mars, and thus subjects the accretion history and isotopic evolution of Mars-sized or smaller bodies to large statistical fluctuations. Performing models ini-tiated with larger numbers of smaller embryos is an obvious future task. Such models could also investigate the effect of a change in equilibration style depending on the relative sizes of impactor and target.

Secondly, we have focused on spatial variations in only one parameter, y, while it is quite likely that the partitioning behaviour (controlled by D) varies in both space and time [3]. Some constraints on the behaviour of D with oxygen fugacity, temperature and pressure are available [50,51]. However, incorporating these effects into a model such as the one presented here would require both the thermal evolution and the volatile history of each body to be modelled. To do so would be a major undertaking; though some preliminary work has been done on thermal evolution ([27,39,69–71], e.g.), the corresponding volatile evolution is less well understood ([72], e.g.). An additional complication is that the extent and timing of initial embryo differentiation may vary with heliocentric distance [34].

Thirdly, we have focused here primarily on a single isotopic system. As noted in Section 4.5, addition of similar isotopic systems with different half-lives will provide important additional constraints [45,73], though some systems (such as U–Pb) can be complicated by additional effects such as volatile loss ([4], e.g.).

Fourthly, the accretion simulations themselves need to be improved. Not only is it desirable to work with smaller initial particles, but the role of dynamical friction due to small bodies [59] and/or nebular gas drag may be crucial in damping the model eccentricities down to the observed levels [57,58]. Both of these effects are also likely to have isotopic consequences: a steady drizzle of (presumably undifferentiated) small bodies on to an accreting planet would drive it towards a more mantle equilibration-like isotopic signature; similarly, nebular gas loss is likely to be associated with general volatile depletion, which in turn affects partitioning behaviour [4]. The collision process is undoubtedly more complicated than the simple mergers assumed here; both fragmentation and inelastic bouncing [74] may result in bodies with distinctive isotopic signatures and iron : silicate ratios. The timing of giant planet formation is also likely to be crucial in determining the growth rates of Mars-like bodies, and the isolation of Vesta-like embryos.

Nonetheless, despite these shortcomings, the agreement between model results and observations suggest that both the dynamical and the isotopic calculations are approximately correct, and that future investigations will provide improved constraints on the physics of large impacts and the early evolution of the inner solar system.

Acknowledgements

We thank Tim Elliott for helpful comments, and Thorsten Kleine for a thorough review. This work was supported by the NASA Origins (FN, CBA) and NASA PG&G (CBA) programs.

References

[1] C.B. Agnor, R.M. Canup, H.F. Levison, On the character and consequence of large impacts in the late stage of terrestrial planet formation, Icarus 142 (1999) 217–237.
[2] J. Chambers, Making more terrestrial planets, Icarus 152 (2001) 205–224.
[3] T. Kleine, K. Mezger, H. Palme, C. Munker, The W isotope evolution of the bulk silicate Earth: constraints on the timing and mechanisms of core formation and accretion, Earth Planet. Sci. Lett. 228 (2004) 109–123.
[4] A.N. Halliday, Mixing, volatile loss and compositional change during impact-driven accretion of the Earth, Nature 427 (2004) 505–509.
[5] S.B. Jacobsen, The Hf–W isotopic system and the origin of the Earth and Moon, Annu. Rev. Earth Planet. Sci. 33 (2005) 531–570.
[6] G.W. Wetherill, Formation of the Earth, Annu. Rev. Earth Planet. Sci. 18 (1990) 205–256.
[7] J. Lissauer, G. Stewart, Growth of planets from planetesimals, in: D. Black, M. Matthews (Eds.), Protostars and Planets, vol. III, Univ. of Arizona Press, 1993, pp. 1061–1088.
[8] S.J. Weidenschilling, Formation of planetesimals and accretion of the terrestrial planets, Space Sci. Rev. 92 (2000) 295–310.
[9] R.M. Canup, C.B. Agnor, Accretion of the terrestrial planets and the Earth–Moon system, in: R.M. Canup, K. Righter (Eds.), Origin of the Earth and Moon, Univ. of Arizona Press, 2000, pp. 113–132.
[10] R. Greenberg, J. Wacker, W.K. Hartmann, C.R. Chapman, Planetesimals to planets: numerical simulations of collisional evolution, Icarus 35 (1978) 1–26.
[11] G.W. Wetherill, G. Stewart, Formation of planetary embryos: effects of fragmentation, low relative velocity, and independent variation of eccentricity and inclination, Icarus 106 (1993) 190–209.
[12] S.J. Weidenschilling, D. Spaute, D.R. Davis, F. Marzari, K. Ohtsuki, Accretional evolution of a planetesimal swarm 2. The terrestrial zone, Icarus 106 (1997) 190–209.
[13] E. Kokubo, S. Ida, Oligarchic growth of protoplanets, Icarus 131 (1998) 171–178.
[14] G.W. Wetherill, An alternative model for the formation of the asteroids, Icarus 100 (1992) 307–325.
[15] J. Chambers, G.W. Wetherill, Making the terrestrial planets: N-body integrations of planetary embryos in three dimensions, Icarus 136 (1998) 304–327.

[16] Q. Yin, S.B. Jacobsen, The ^{97}Tc ^{97}Mo chronometer and its implications for timing of terrestrial accretion and core formation, Lunar Planet. Sci. Conf., XXIX:Abs, vol. 1802, 1998.
[17] R.W. Carlson, E.H. Hauri, Extending the Pd-107–Ag-107 chronometer to low Pd/Ag meteorites with multicollector plasma-ionization mass spectrometry, Geochim. Cosmochim. Acta 65 (2001) 1839–1848.
[18] D.-C. Lee, A.N. Halliday, Hafnium–tungsten chronometry and the timing of terrestrial core formation, Nature 378 (1995) 771–774.
[19] T. Kleine, C. Munker, K. Mezger, H. Palme, Rapid accretion and early core formation on asteroids and the terrestrial planets from Hf–W chronometry, Nature 418 (2002) 952–955.
[20] Q. Yin, S.B. Jacobsen, K. Yamashita, J. Blichert-Toft, P. Telouki, F. Albarede, A short timescale for terrestrial planet formation from Hf–W chronometry of meteorites, Nature 418 (2002) 949–952.
[21] R. Schoenberg, B.S. Kamber, K.D. Collerson, O. Eugster, New W-isotope evidence for rapid terrestrial accretion and very early core formation, Geochim. Cosmochim. Acta 66 (17) (2002) 3151–3160.
[22] T. Kleine, C. Munker, K. Mezger, H. Palme, A. Bischo, 182Hf–182W isotope systematics of chondrites, eucrites, and martian meteorites: chronology of core formation and early mantle differentiation in Vesta and Mars, Geochim. Cosmochim. Acta 68 (13) (2004) 2935–2946.
[23] D.J. Stevenson, Fluid dynamics of core formation, in: H.E. Newsom, J.E. Jones (Eds.), Origin of the Earth, Oxford Univ. Press, 1990, pp. 231–249.
[24] T. Yoshino, M.J. Walter, T. Katsura, Connectivity of molten Fe alloy in peridotite based on in situ electrical conductivity measurements: implications for core formation in terrestrial planets, Earth Planet. Sci. Lett. 222 (2) (2004) 625–643.
[25] M.C. Shannon, C.B. Agee, Percolation of core melts at lower mantle conditions, Science 280 (5366) (1998) 1059–1061.
[26] D. Bruhn, N. Groebner, D.L. Kohlstedt, An interconnected network of core-forming melts produced by shear deformation, Nature 403 (6772) (2000) 883–886.
[27] H. Senshu, K. Kuramoto, T. Matsui, Thermal evolution of a growing Mars, J. Geophys. Res. 107 (E12) (2002) doi:10.1029/2001JE001819.
[28] R. Merk, D. Breuer, T. Spohn, Numerical modeling of ^{26}Al-induced radioactive melting of asteroids considering accretion, Icarus 159 (2002) 183–191.
[29] A. Ghosh, H.Y. McSween, A thermal model for the differentiation of asteroid 4 Vesta, based on radiogenic heating, Icarus 134 (1998) 187–206.
[30] G. Srinivasan, J.N. Goswami, N. Bhandari, Al-26 in eucrite piplia kalan: plausible heat source and formation chronology, Science 284 (5418) (1999) 1348–1350.
[31] G.W. Lugmair, A. Shukolyukov, Early solar system timescales according to 53Mn–53Cr systematics, Geochim. Cosmochim. Acta 62 (16) (1998) 2863–2886.
[32] R.W. Carlson, G.W. Lugmair, Timescales of planetesimal formation and differentiation based on extinct and extant radioisotopes, in: R.M. Canup, K. Righter (Eds.), Origin of the Earth and Moon, Univ. of Arizona Press, 2000, pp. 25–44.
[33] M.F. Horan, M.I. Smoliar, R.J. Walker, W-182 and re-187–os-187 systematics of iron meteorites: chronology for melting, differentiation, and crystallization in asteroids, Geochim. Cosmochim. Acta 62 (3) (1998) 545–554.
[34] R.E. Grimm, H.Y. McSween, Heliocentric zoning of the asteroid belt by aluminum-26 heating, Science 259 (5095) (1985) 653–655.
[35] D.J. Stevenson, Formation and early evolution of the Earth, in: W.R. Peltier (Ed.), Mantle Convection and Plate Tectonics, Gordon and Breach, 1989, pp. 818–868.
[36] W.M. Kaula, Thermal evolution of Earth and Moon growing by planetesimal impacts, J. Geophys. Res. 84 (1979) 999–1008.
[37] G.F. Davies, Heat deposition and retention in a solid planet growing by impacts, Icarus 63 (1985) 45–68.
[38] S.W. Squyres, R.T. Reynolds, A.L. Summers, F. Shung, Accretional heating of the satellites of Saturn and Uranus, J. Geophys. Res. 93 (B8) (1988) 8779–8794.
[39] W.B. Tonks, H.J. Melosh, Magma ocean formation due to giant impacts, J. Geophys. Res. — Planets 98 (E3) (1993) 5319–5333.
[40] K. Righter, M.J. Drake, Core formation in Earth's Moon, Mars and Vesta, Icarus 124 (1996) 513–529.
[41] S.I. Karato, V.R. Murthy, Core formation and chemical equilibrium in the Earth- I. Physical considerations, Phys. Earth Planet. Inter. 100 (1997) 61–79.
[42] D.C. Rubie, H.J. Melosh, J.E. Reid, C. Liebske, K. Righter, Mechanisms of metal–silicate equilibration in the terrestrial magma ocean, Earth Planet. Sci. Lett. 205 (2003) 239–255.
[43] R.M. Canup, Simulations of a late lunar-forming impact, Icarus 168 (2004) 433–456.
[44] H.J. Melosh, Impact Cratering: A Geologic Process, Oxford Univ. Press, New York, 1989.
[45] C.L. Harper, S.B. Jacobsen, Evidence for 182Hf in the early Solar System and constraints on the timescale of terrestrial accretion and core formation, Geochim. Cosmochim. Acta 60 (7) (1996) 1131–1153.
[46] Y.X. Zhang, The age and accretion of the Earth, Earth Sci. Rev. 59 (1–4) (2002) 235–263.
[47] A.G.W. Cameron, W. Benz, The origin of the Moon and the single impact hypothesis IV, Icarus 92 (1991) 204–216.
[48] R.M. Canup, W.R. Ward, A.G.W. Cameron, A scaling relationship for satellite-forming impacts, Icarus 150 (2) (2001) 288–296.
[49] A.F. Nelson, W. Benz, F.C. Adams, D. Arnett, Dynamics of circumstellar disks, Astrophys. J. 502 (1998) 342–371.
[50] K. Righter, Metal–silicate partitioning of siderophile elements and core formation in the early Earth, Annu. Rev. Earth Planet. Sci. 31 (2003) 135–174.
[51] M.J. Walter, H.E. Newsom, W. Ertel, A. Holzheid, Siderophile elements in the Earth and Moon: metal/silicate partitioning and implications for core formation, in: R.M. Canup, K. Righter (Eds.), Origin of the Earth and Moon, Univ. Ariz. Press, 2000, pp. 265–289.
[52] A.N. Halliday, D.-C. Lee, S.B. Jacobsen, Tungsten isotopes, the timing of metal–silicate fractionation, and the origin of the Earth and Moon, in: R.M. Canup, K. Righter (Eds.), Origin of the Earth and Moon, Univ. Ariz. Press, 2000, pp. 45–62.
[53] H.E. Newsom, K.W.W. Sims, P.D. Noll, W.L. Jaeger, S.A. Maehr, T.B. Beserra, The depletion of tungsten in the bulk silicate earth: constraints on core formation, Geochim. Cosmochim. Acta 60 (7) (1996) 1155–1169.
[54] K. Lodders, B. Fegley, In The Planetary Scientist's Companion, Oxford University press, New York, 1998.
[55] C.L. Harper, L.E. Nyquist, B. Bansal, H. Wiesmann, C.Y. Shih, Rapid accretion and early differentiation of Mars indicated by Nd-142 Nd-144 in SNC meteorites, Science 267 (5195) (1995) 213–217.
[56] D.C. Lee, A.N. Halliday, I. Leya, R. Wieler, U. Wiechert, Cosmogenic tungsten and the origin and earliest differentiation of the moon, Earth Planet. Sci. Lett. 198 (2002) 267–274.

[57] C.B. Agnor, W.R. Ward, Damping of terrestrial-planet eccentricities by density–wave interactions with a remnant gas disk, Astrophys. J. 567 (2002) 579–586.
[58] J. Kominami, S. Ida, The effect of tidal interaction with a gas disk on formation of terrestrial planets, Icarus 157 (2002) 43–56.
[59] H. Levison, D. Nesvorny, C. Agnor, A. Morbidelli, The Role of Dynamical Friction in Terrestrial Planet Formation. AAS/Division for Planetary Sciences Meeting Abstracts, 37:−+, August 2005.
[60] W. Benz, A.G.W. Cameron, W.L. Slattery, Collisional stripping of mercury's mantle, Icarus 74 (1987) 516–528.
[61] K.K. Turekian, S.P. Clark, Inhomogeneous accumulation of the earth from the primitive solar nebula, Earth Planet. Sci. Lett. 6 (1969) 346–348.
[62] G.W. Wetherill, Provenance of the terrestrial planets, Geochmi. Cosmochim. Acta 58 (1994) 4513–4520.
[63] A. Morbidelli, J. Chambers, J.I. Lunine, J.M. Petit, F. Robert, G.B. Valsecchi, K.E. Cyr, Source regions and timescales for the delivery of water to the Earth, Meteorit. Planet. Sci. 35 (2000) 1309–1320.
[64] S.N. Raymond, T. Quinn, J.I. Lunine, Making other earths: dynamical simulations of terrestrial planet formation and water delivery, Icarus 168 (2004) 1–17.
[65] U. Wiechert, A.N. Halliday, D.C. Lee, G.A. Snyder, L.A. Taylor, D. Rumble, Oxygen isotopes and the moon-forming giant impact, Science 294 (2001) 345–348.
[66] F. Nimmo, K. Tanaka, Early crustal evolution of Mars, Annu. Rev. Earth Planet. Sci. 33 (2005) 133–161.
[67] D.E. Wilhelms, S.W. Squyres, The Martian hemispheric dichotomy may be due to a giant impact, Nature 309 (5964) (1984) 138–140.
[68] S.J. Woodland, M. Rehkamper, A.N. Halliday, D.C. Lee, B. Hattendorf, D. Gunther, Accurate measurement of silver isotopic compositions in geological materials including low pd/ag meteorites, Geochim. Cosmochim. Acta 69 (8) (2005) 2153–2163.
[69] H.J. Melosh, Giant impacts and the thermal state of the early Earth, in: H.E. Newsom, J.E. Jones (Eds.), Origin of the Earth, Oxford Univ. Press, 1990, pp. 69–83.
[70] R.M. Canup, E. Asphaug, Origin of the Moon in a giant impact near the end of the Earth's formation, Nature 412 (2001) 708–712.
[71] C.C. Reese, V.S. Solomatov, J.R. Baumgardner, Survival of impact-induced thermal anomalies in the Martian mantle, J. Geophys. Res. 107 (E10) (2002) art. no. 5082.
[72] A.N. Halliday, D. Porcelli, In search of lost planets: the paleocosmochemistry of the inner solar system, Earth Planet. Sci. Lett. 192 (4) (2001) 545–559.
[73] C.J. Allegre, G. Manhes, C. Gopel, The age of the Earth, Geochim. Cosmochim. Acta 59 (1995) 1445–1456.
[74] C.B. Agnor, E. Asphaug, Accretion efficiency during planetary collisions, Astrophys. J. 613 (2004 (October)) L157–L160.